Journal of Power Sources 193 (2009) 816–821

Contents lists available at ScienceDirect

Journal of Power Sources

journal homepage: www.elsevier.com/locate/jpowsour

Preparation and electrochemical properties of $Li_4Ti_5O_{12}$ thin film electrodes by pulsed laser deposition

Jianqiu Deng[a], Zhouguang Lu[a], I. Belharouak[b], K. Amine[b], C.Y. Chung[a,*]

[a] Department of Physics & Materials Science, City University of Hong Kong, Tat Chee Avenue, Kowloon, Hong Kong, China
[b] Argonne National Laboratory, Chemical Engineering Division, Argonne, IL 60439, USA

ARTICLE INFO

Article history:
Received 19 November 2008
Received in revised form 25 March 2009
Accepted 30 March 2009
Available online 18 April 2009

Keywords:
Rechargeable lithium-ion battery
Lithium titanate thin film
Anode
Pulsed laser deposition

ABSTRACT

Spinel $Li_4Ti_5O_{12}$ thin film anode material for lithium-ion batteries is prepared by pulsed laser deposition. Thin film anodes are deposited at ambient temperature, then annealed at three different temperatures under an argon gas flow and the influence of annealing temperatures on their electrochemical performances is studied. The microstructure and morphology of the films are characterized by XRD, SEM and AFM. Electrochemical properties of the films are evaluated by using galvanostatic discharge/charge tests, cyclic voltammetry and a.c. impedance spectroscopy. The results reveal that all annealed films crystallize and exhibit good cycle performance. The optimum annealing temperature is about 700 °C. The steady-state discharge capacity of the films is about 157 mAh g^{-1} at a medium discharge/charge current density of 10 μA cm^{-2}. At a considerably higher discharge/charge current density of 60 μA cm^{-2} (about 3.45 C) the discharge capacity of the films remains steady at a relative high value (146 mAh g^{-1}). The cycleability of the films is excellent. This implies that such films are suitable for electrodes to be used at high discharge/charge current density.

1. Introduction

Spinel lithium titanate $Li_4Ti_5O_{12}$ has attracted great attention as a negative electrode (anode) material for rechargeable lithium batteries because of the following attributes: 'zero-strain' effect, flat Li insertion voltage, excellent reversibility during charge–discharge cycles, and good safety characteristics [1,2]. At 1.55 V, three lithium ions per formula unit can be inserted into $Li_4Ti_5O_{12}$ to give a theoretical capacity of 175 mAh g^{-1}. One of the drawbacks of $Li_4Ti_5O_{12}$ is the poor electrical conductivity which prohibits it from wide practical application.

Thin film electrodes are useful for the investigation of the electrochemical properties of active materials that have poor conductivity. The thickness of thin films can be reduced to a value at which the electrical conductivity does not significantly affect the electrochemical behaviour [3]. Recently, $Li_4Ti_5O_{12}$ thin films for lithium-ion battery electrodes prepared by the spray pyrolysis technique, the sol–gel method, the radio frequency (RF) magnetron sputtering technique or the electrostatic spray deposition technique have been reported [4–7].

Pulsed laser deposition (PLD) technique is one of the more beneficial methods for the growth of materials containing volatile components with complex stoichiometries. The technique has many advantages over other deposition methods, such as high deposition rate, precise control over film thickness, and less deviation from the target composition [8,9]. By using PLD technique, layered phase $LiCoO_2$ and spinel phase $LiMn_2O_4$ cathodes with high charge voltage and cycling stability for lithium-ion batteries have been successfully prepared [10–13]. $LiCoO_2$ and $LiFePO_4$/Ag thin film electrode materials have also been prepared by PLD technique [14,15].

In this investigation, $Li_4Ti_5O_{12}$ thin films are prepared via the PLD technique. The effect of annealing temperature on their electrochemical performance is investigated. The best annealing temperature is around 700 °C, which produces an anode material with high capacity and good cycle performances.

2. Experimental

2.1. Preparation of the $Li_4Ti_5O_{12}$ thin film

$Li_4Ti_5O_{12}$ thin films were deposited on Pt/Ti/SiO_2/Si substrates (supplied by the Institute of Microelectronics, Peking University) at ambient temperature in an argon atmosphere of 6 Pa for 40 min by PLD with a stoichiometric $Li_4Ti_5O_{12}$ target. The thickness of Pt current-collector layer and the Ti buffer layer was 150 and 100 nm, respectively. The target was prepared from pure $Li_4Ti_5O_{12}$ powder mixed with an appropriate amount of polyvinyl alcohol (PVA)

* Corresponding author.
E-mail address: appchung@cityu.edu.hk (C.Y. Chung).

0378-7753/$ – see front matter © 2009 Elsevier B.V. All rights reserved.
doi:10.1016/j.jpowsour.2009.03.074

and then dried at 80 °C for 12 h. The dried powders were ground thoroughly and pressed into pellet at a pressure of 392 MPa. Subsequently, the pellet was sintered at 950 °C for 6 h in air to yield a $Li_4Ti_5O_{12}$ target with a density about 90% of that of dense $Li_4Ti_5O_{12}$ (3.5 g cm^{-3}).

A Lambda Physik LPX 200 KrF excimer laser beam (248 nm, 250 mJ) was used for deposition with laser pulse frequency of 10 Hz. The distance between the target and substrate was kept at 4 cm. Both of the target and substrate holder were rotated continuously to ensure uniform deposition of the anode film. Prior to deposition, the vacuum PLD chamber was evacuated to a background pressure of 1.3×10^{-3} Pa. The as-deposited thin films were then annealed at various temperatures for 30 min in a quartz tube. The pressure inside the quartz tube was maintained at 13 Pa by purging pure Ar gas before increasing the temperature.

2.2. Physical characterization

X-ray diffraction (XRD) analyses of the anode films were carried out with a SIEMENS D500 diffractometer with Cu Kα radiation at room temperature. Data were collected in the 2θ range of 10–90° at a scan rate of 0.02° s^{-1}. The surface morphology and cross-section of each film were examined by scanning electron microscopy (SEM, Joel JSM-820) and atom force microscopy (AFM, Thermomicroscope CP Research scanning probe microscope).

2.3. Electrochemical characterization

The electrochemical properties of $Li_4Ti_5O_{12}$ thin films were investigated by cyclic voltammetry (CV) and galvanostatic discharge/charge tests. The geometric electrode area was 1 cm^2. A three-electrode cell with lithium metal foil as the counter and reference electrodes was used in the electrochemical characterization. All experiments were conducted in an Ar-filled glove box in which the O_2 level was kept below 0.1 ppm. The electrolyte was 1 M $LiClO_4$ in propylene carbonate (PC) (battery grade, water content: 30 ppm). The electrochemical properties of the anode film were characterized by means of an automatic Versa-Stat EG&G system. Cyclic voltammetry was conducted between 1.0 and 2.0 V versus Li/Li^+ at different scan rates. Galvanostatic discharge–charge cycle tests were performed between 1.0 and 2.0 V using different fixed current densities. Analysis by a.c. impedance spectroscopy was carried out in the frequency range of 100 mHz–100 kHz with a CHI-660C electrochemical workstation. The a.c. amplitude was 5 mV with an open-circuit potential of 1.56 V.

3. Results and discussions

3.1. X-ray diffraction

A main peak corresponding to the plane (1 1 1) was observed in the XRD spectra of the films annealed at 600, 700, and 800 °C for 30 min. This indicates that the $Li_4Ti_5O_{12}$ films grown on the $Pt/Ti/SiO_2/Si$ substrates have a spinel type structure and the preferred plane is (1 1 1). The XRD patterns of the $Li_4Ti_5O_{12}$ target and the anode film annealed at 800 °C are shown in Fig. 1. The major peaks corresponding to the planes (2 2 2), (3 3 3) and (4 4 4) are relatively low, see Fig. 1(a). The average lattice constant of the $Li_4Ti_5O_{12}$ films calculated from the XRD peaks is 8.375 Å. The value is slightly larger than that of bulk $Li_4Ti_5O_{12}$ (8.359 Å) [1]. It has been reported that the average lattice constant of thin films prepared by the RF magnetron sputtering technique is less than that of bulk $Li_4Ti_5O_{12}$ [7]. Full width at half-maximum (FWHM) of the strongest peak, i.e. (1 1 1) plane, is 0.331°, 0.314° and 0.303° for thin films annealed at 600, 700 and 800 °C, respectively. According to the inverse relationship between FWHM and grain size, this implies that the grain size is larger with increase in annealed temperature. This is consistent with the SEM and AFM results. Similar results have also been reported by other researchers [5].

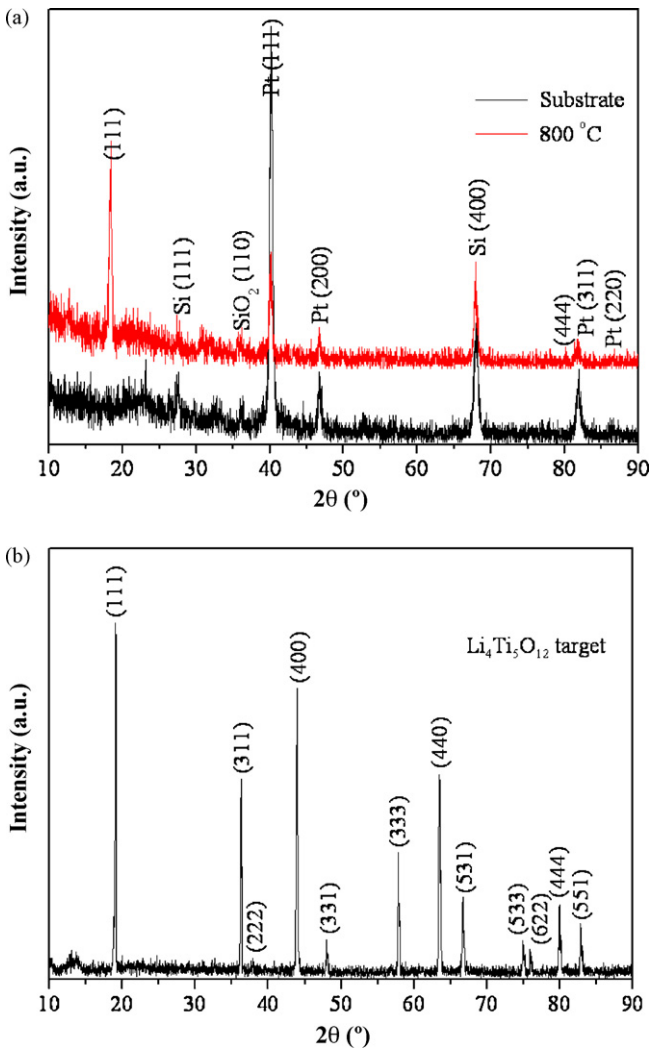

Fig. 1. XRD spectrum of $Li_4Ti_5O_{12}$ thin film and target: (a) thin film deposited on $Pt/Ti/SiO_2/Si$ and annealed at 800 °C; (b) corresponding target material.

3.2. Scanning electron microscopy and atom force microscopy

Scanning electron micrographs of the $Li_4Ti_5O_{12}$ films annealed at different temperatures are shown in Fig. 2. The micrographs reveal that the films exhibit different surface roughness and dispersed island-like grains. The grain size is larger with increase in annealing temperature. The SEM images of the cross-section of the films are shown in Fig. 2(c–e). Films annealed at 700 °C or above exhibit a disordered porous morphology composed of individual nanoparticles with a narrow size-distribution, as evidenced by the film annealed at 800 °C (Fig. 2(e)). The cross-section images reveal that the thickness is about 230, 290 and 410 nm for the thin films annealed at 600, 700 and 800 °C, respectively. This can be attributed to a transformation to a porous structure on high temperature annealing (Fig. 2(e)).

Atom force microscopic analysis also reveals a rough morphology. Typical three-dimensional AFM images of the surface topography of $Li_4Ti_5O_{12}$ thin films annealed at 700 and 800 °C are given in Fig. 3. The $Li_4Ti_5O_{12}$ thin film annealed at 700 °C, as shown in Fig. 3(a), has relatively smaller grains and a slightly rougher sur-

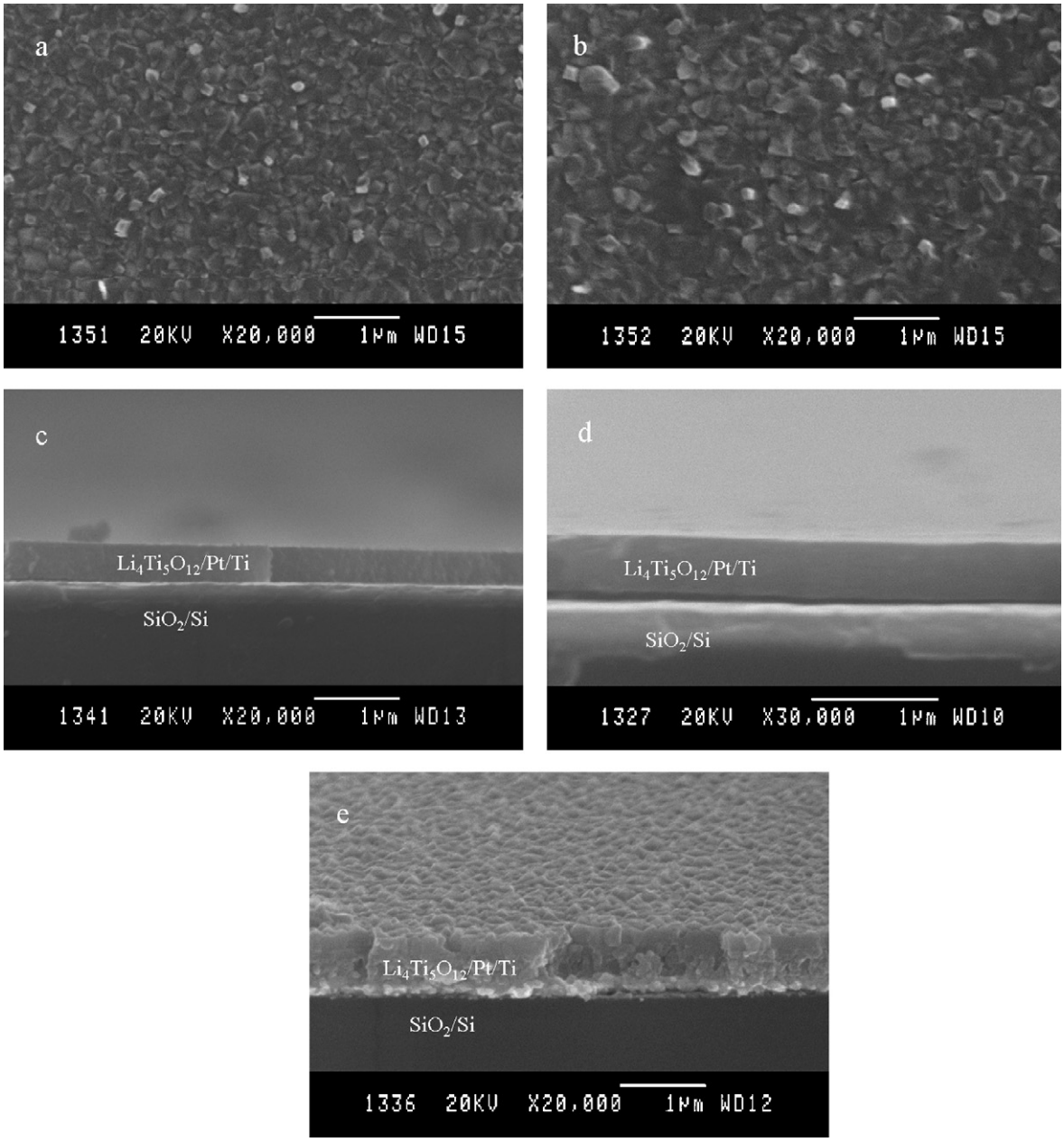

Fig. 2. SEM images of $Li_4Ti_5O_{12}$ thin films annealed at different temperature. (a) Surface image of film annealed at 700 °C, (b) surface image of film annealed at 800 °C, (c) cross-section image of film annealed at 600 °C, (d) cross-section image of film annealed at 700 °C, and (e) cross-section image of film annealed at 800 °C.

face. For the 800 °C annealed film (Fig. 3(b)), larger and coarser grains with a much rougher surface are obtained. This is consistent with the XRD and SEM results. The surface root-mean-square (rms) roughness determined from randomly selected regions is 24 and 39 nm for the thin films annealed at 700 and 800 °C, respectively.

3.3. Electrochemical properties

The electrochemical properties of the films annealed at various temperatures were evaluated with CV at scan rates of 0.1, 0.5, 1 and 5 mV s^{-1}. The cyclic voltammograms of the thin films annealed at 600–800 °C are presented in Fig. 4. A couple of anodic and cathodic sharp peaks can be found in all films; no other redox peaks are present. This indicates that all the films are pure $Li_4Ti_5O_{12}$ which shows good reversible redox reactions. The reversibility of redox reaction is the best for the film annealed at 700 °C. The pair of redox reaction peaks located between 1.5 and 1.6 V at a scan rate of 0.1 mV s^{-1} is characteristic of electrochemical lithium insertion/extraction of $Li_4Ti_5O_{12}$ [5,7]. The oxidation/reduction peak currents increase with increasing scan rate (Fig. 4(b)). The oxidation peaks shift to higher potentials, while the reduction peaks shift to lower potentials. The cathodic and anodic peaks located between 1.5 and 1.6 V correspond to the potential plateaux of the discharge and charge process, respectively, in which Li intercalate/de-intercalate into/out of the spinel $Li_4Ti_5O_{12}$. The difference between the oxidation and reduction peak potentials is 73 mV for thin films annealed at 700 °C; a value which is larger than the results obtained by other authors [5,7] but is smaller than that reported by Yu et al. [6]. The discrepancy in the results may be attributed to the variation of lithium-ion diffusivity in different $Li_4Ti_5O_{12}$ thin films with different morphology and thickness as a result of different deposition methods.

Discharge–charge curves of the films between 1.0 and 2.0 V are shown in Fig. 5. A pair of flat discharge–charge potential plateaux

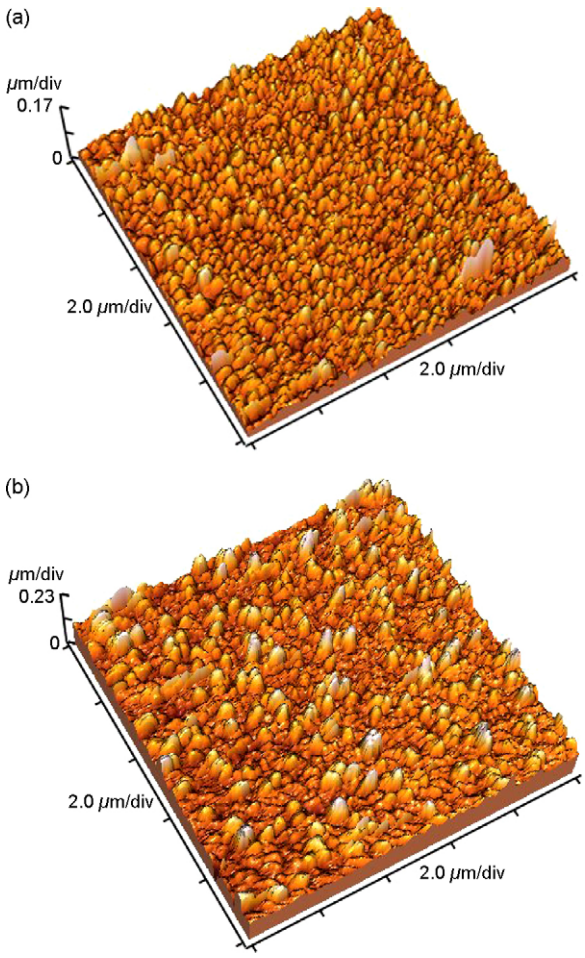

Fig. 3. AFM images of surface topography of $Li_4Ti_5O_{12}$ thin films deposited on $Pt/Ti/SiO_2/Si$ substrates: (a) annealed at 700 °C; (b) annealed at 800 °C.

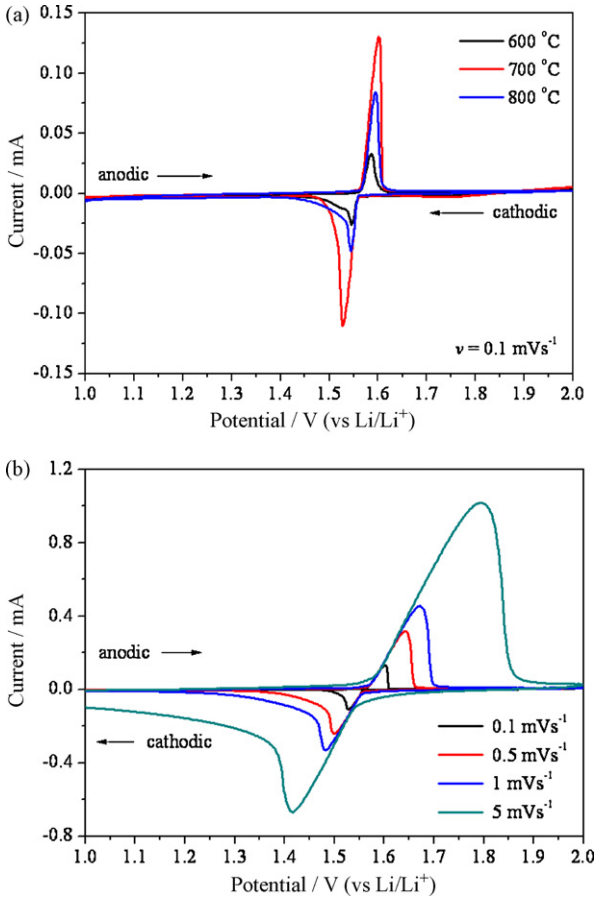

Fig. 4. Cyclic voltammograms of anode films: (a) annealed at 600, 700 and 800 °C, $V = 0.1$ mV s^{-1}; (b) annealed at 700 °C, at different scan rates of 0.1, 0.5, 1 and 5 mV s^{-1}.

around 1.55 and 1.58 V corresponds to the sharp redox peaks in Fig. 4(a). The discharge capacity for the films annealed at 700 °C is the largest when tested at a constant current density of 20 μA cm^{-2} (see Fig. 5(a)). This finding is consistent with the cyclic voltammetric data, where the capacity is the largest for the film annealed at 700 °C. The discharge capacity obtained at 20 μA cm^{-2} for the film annealed at 700 °C is larger than that of the film annealed at 600 °C. This result can be attributed to higher crystallinity after 700 °C annealing.

By contrast, the discharge capacity of the film annealed at 800 °C is smaller than that at 700 °C. This result can be explained by a difference in the adhesion strength [5] between the films and the substrates. The grain size increases with higher annealing temperature and will therefore lead to a larger surface area by forming the disordered porous morphology. This feature is favourable for the Li^+ ion intercalation and de-intercalation process due to the larger contact area with the liquid electrolyte. On the other hand, relatively smaller grains usually provide good electronic conductivity, which decreases the diffusion distance of the Li^+ ions in the active material and also reduces the charge-transfer resistance at the electrode|electrolyte interface. Larger grain size may also lead to higher mechanical stress during the Li^+ ion intercalation and de-intercalation processes, and thereby result in easy detachment of the film from the substrate.

Typical discharge–charge curves of the films annealed at 700 °C and tested at different current densities are presented in Fig. 5(b). When the current density is increased, the discharge/charge capacity decrease initially and at the same time the discharge/charge overpotential becomes more pronounced. When the current density is high, e.g., 60 μA cm^{-2} (about 3.45 C), the discharge and charge capacities increase. The relative larger discharge and charge capability at a high rate (60 μA cm^{-2}) discharge–charge process is considered to be mainly due to the fast ionic diffusion kinetics resulting from the small grain size and the porous structure.

The first discharge and charge capacity is approximately 149 and 146 mAh g^{-1} (calculated using a theoretical density of 3.5 g cm^{-3}) at the flat potential plateaux of 1.54 and 1.58 V at a constant current density of 10 μA cm^{-2}, as shown in Fig. 5(c). The discharge capacity is slightly smaller than that reported for films grown by the RF magnetron sputtering technique [7]. The irreversible capacity loss on the first cycle is about 2.9 mAh g^{-1}. This loss may be due to the growth of a surface passivation layer that blocks the charge-transfer reaction between the anode and the electrolyte during discharge–charge cycle [16].

The cycle performance between 1.0 and 2.0 V at a constant current density of 20 μA cm^{-2} is good for all the films, as shown in Fig. 6(a). This can be attributed to the good crystallinity of the films, the stability of the spinel crystal structure, and the zero-strain insertion reaction of $Li_4Ti_5O_{12}$ upon discharge–charge cycling [1,17]. As mentioned above, the steady-state discharge capacity of the film annealed at 700 °C is the largest for all the films. The difference in discharge capacity of these films could be due to the effects of crystallinity, grain size, and the adhesion between the anode films and the substrates. These factors lead to differences in lithium ion diffusion length, as well as in the mechanical stress related to the Li^+ ion intercalation and de-intercalation process.

The discharge capacity versus cycle number of the 700 °C annealed thin film characterized at different current densities

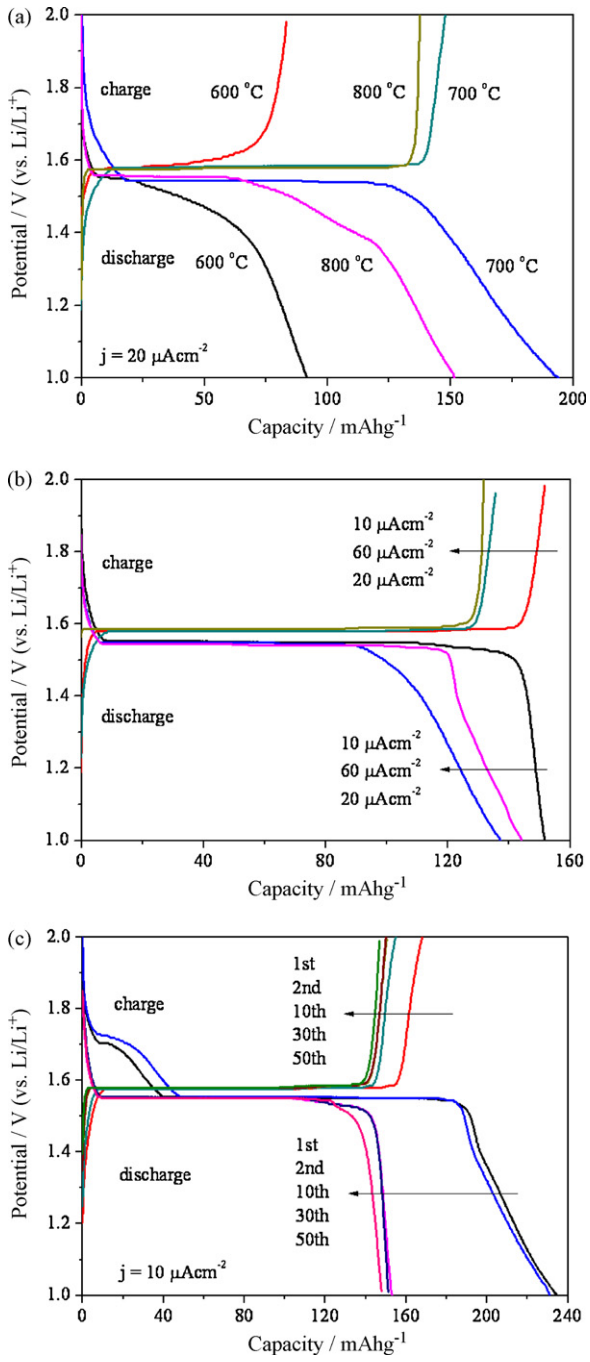

Fig. 5. Discharge–charge curves of $Li_4Ti_5O_{12}$ thin films: (a) annealed at various temperatures at a constant current density of 20 μA cm^{-2}; (b) annealed at 700 °C at various current densities (10–60 μA cm^{-2}); (c) annealed at 700 °C and then cycled at constant current density of 10 μA cm^{-2}. Curves measured between 1.0 and 2.0 V.

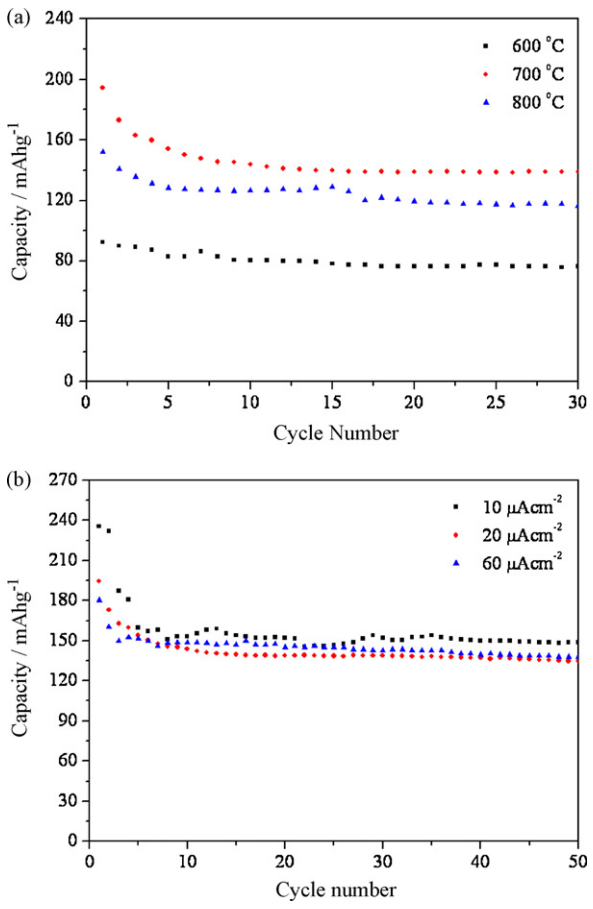

Fig. 6. Discharge capacity versus cycle number of $Li_4Ti_5O_{12}$ thin films: (a) annealed at various temperatures at constant current density of 20 μA cm^{-2} between 1.0 and 2.0 V; (b) annealed at 700 °C at different current densities.

between 1.0 and 2.0 V is shown in Fig. 6(b). The anode film shows excellent electrochemical performances. The shape of the curves and their invariance on cycling are in good agreement with previous results [18–20]. The discharge capacity reaches a steady-state value of 157 mAh g^{-1} at constant current density of 10 μA cm^{-2} (i.e. ~0.58 C) after 10 cycles. After 50 cycles, the discharge capacity is 149 mAh g^{-1}, which is 95 cap.% (cap. denotes capacity) of that of the 10th cycle. When the current density is increased, the capacities of anode films decline of slowly. The discharge capacity is lowered to 140 mAh g^{-1} when the current density is increased to 20 μA cm^{-2} (i.e. ~1.15 C). Nevertheless, the performance of the film is still good upon cycling. At a higher current density of 60 μA cm^{-2} (i.e. ~3.45 C), the steady-state discharge capacity is about 146 mAh g^{-1}, which is about 4 cap.% higher than that at the 1.15 C rate. The film maintains excellent cycleability, although the capacity fades faster than that of the 0.58 and 1.15 C cycled specimens.

The dependence of the capacity with respect to current density can be explained as follows. At a slower rate, lithium ions have more time to diffuse into the film interior so that the capacity at low current density is not diffusion-limited. When current density is increased to higher values, the excellent high-rate performance appears to be ascribed to the porous morphology. The porous structure consists of nanoparticles that are in intimate contact and there are many pores. The structure therefore offers better electrical conduction and a larger electrode|electrolyte interface, which are important in improving the ionic diffusion kinetics and result in superior electrochemical performance. Good high-rate performance with high capacities and high capacity retention have also been reported in the literature for such a structure [19,21,22].

The a.c. impedance spectrum at a half-discharged state and an open-circuit potential of 1.56 V indicates that the impedance of thin films is rather high, which is due to the poor electrical conductivity of $Li_4Ti_5O_{12}$. The a.c. impedance spectrum of the film annealed in 700 °C is shown in Fig. 7. It is composed of a slightly depressed semicircle at high frequency (100 kHz–81.38 Hz), a straight line in the medium-frequency Warburg region (81.38–0.8071 Hz), and a steep sloping line in the low-frequency region (0.8071 Hz–100 mHz). Cole–Cole plots of similar shape have been obtained for $LiCoO_2$ films [11] and $Li_4Ti_5O_{12}$ films [5,6]. The semicircle at high frequency is due to the charge-transfer resistance related to interfacial Li^+

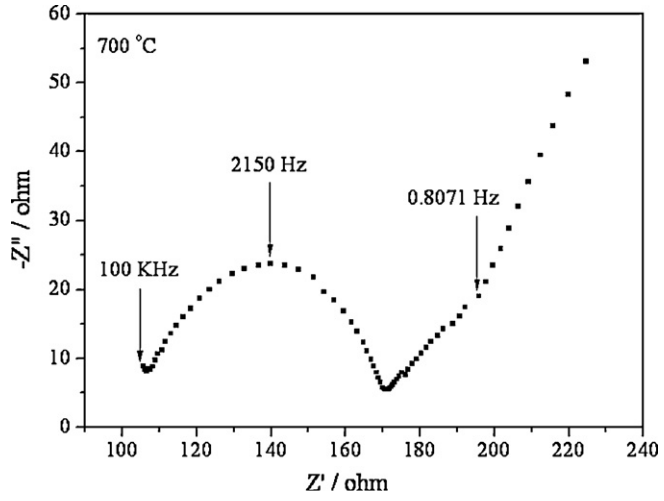

Fig. 7. a.c. impedance plot of film annealed at 700 °C.

ion transfer; the diameter of semicircle corresponds to the charge-transfer resistance. The medium-frequency Warburg region and low-frequency region are attributed to solid-state diffusion of Li^+ ion. The chemical diffusion coefficient can be determined from [23]:

$$D = \frac{\pi f l^2}{1.94} \quad (1)$$

where f is transition frequency, l is the thickness of the material or film, and D is the chemical diffusion coefficient. The chemical diffusion coefficient determined using Eq. (1) is $1.1 \times 10^{-9}\ cm^2\ s^{-1}$. The value is in good agreement with that obtained from electrochemical impedance spectroscopy (EIS) analysis [5].

4. Conclusions

Pure spinel structure $Li_4Ti_5O_{12}$ thin film electrodes have been successfully deposited by PLD technique and annealed at various temperatures. The microstructure and electrochemical properties have been investigated. The films annealed at temperatures above 600 °C are crystalline and show a pair of sharp redox reaction peaks between 1.5 and 1.6 V in cyclic voltammograms, which is a characteristic of typical electrochemical lithium insertion/extraction reactions of $Li_4Ti_5O_{12}$. Galvanostatic discharge–charge tests show that all the $Li_4Ti_5O_{12}$ anode films have a stable discharge/charge voltage plateau of 1.54/1.58 V and excellent cycle performance. With increase in the annealing temperature, the films have better crystallinity and larger grain size which result in a large surface area, that favours better electrochemical performance. Unfortunately, the increment in grain size also leads to higher charge transfer-resistance and poorer adhesion. As a consequence, the electrochemical performance is inferior when the annealing temperature is higher than 700 °C. The steady-state discharge capacity between 1.0 and 2.0 V of the film annealed at 700 °C are 157 and 146 mAh g^{-1} at current densities of 10 and 60 μA cm^{-2}, respectively. Compared with the 10th cycle, the discharge capacity remains at 95 cap.% after 50 cycles. These results suggest that $Li_4Ti_5O_{12}$ thin films deposited on $Pt/Ti/SiO_2/Si$ substrates by the PLD technique are promising anodes for application in lithium-ion battery systems.

References

[1] T. Ohzuku, A. Ueda, N. Yamamoto, J. Electrochem. Soc. 142 (1995) 1431.
[2] I. Belharouak, Y.-K. Sun, W. Lu, K. Amine, J. Electrochem. Soc. 154 (2007) A1083.
[3] C. Yada, Y. Iriyama, S.-K. Jeong, T. Abe, M. Inaba, Z. Ogumi, J. Power Sources 146 (2005) 559.
[4] T. Brousse, P. Fragnaud, R. Marchand, D.M. Schleich, O. Bohnke, K. West, J. Power Sources 68 (1997) 412.
[5] Y.H. Rho, K. Kanamura, J. Electrochem. Soc. 151 (2004) A106.
[6] Y. Yu, J.L. Shui, C.H. Chen, Solid State Commun. 135 (2005) 485.
[7] C.-L. Wang, Y.C. Liao, F.C. Hsu, N.H. Tai, M.K. Wu, J. Electrochem. Soc. 152 (2005) A653.
[8] C.V. Ramana, K. Zaghib, C.M. Julien, J. Power Sources 159 (2006) 1310.
[9] N. Ohta, K. Takada, M. Osada, L.Q. Zhang, T. Sasaki, M. Watanabe, J. Power Sources 146 (2005) 707.
[10] C. Julien, M.A. Camacho-Lopez, L. Escobar-Alarcon, E. Haro-Poniatowski, Mater. Chem. Phys. 68 (2001) 210.
[11] S.B. Tang, M.O. Lai, L. Lu, J. Alloys Compd. 449 (2008) 300.
[12] C.Y. Ouyang, H.D. Deng, Z.Q. Ye, M.S. Lei, L.Q. Chen, Thin Solid Films 503 (2006) 268.
[13] I. Yamada, T. Abe, Y. Iriyama, Z. Ogumi, Electrochem. Commun. 5 (2003) 502.
[14] Y. Zhang, C.Y. Chung, L.X. Sun, M. Zhu, Mater. Chem. Phys. 107 (2008) 254.
[15] Z.G. Lu, H. Cheng, M.F. Lo, C.Y. Chung, Adv. Funct. Mater. 17 (2007) 3885.
[16] J. Li, Y.L. Jin, X.G. Zhang, H. Yang, Solid State Ionics 178 (2007) 1590.
[17] K. Zaghib, K. Kinoshita, J. Power Sources 125 (2004) 214.
[18] J. Gao, C.Y. Jiang, J.R. Ying, C.R. Wan, J. Power Sources 155 (2006) 364.
[19] E.M. Sorensen, S.J. Barry, H.-K. Jung, J.R. Rondinelli, J.T. Vaughey, K.R. Poeppelmeier, Chem. Mater. 18 (2006) 482.
[20] X.L. Yao, S. Xie, H.Q. Nian, C.H. Chen, J. Alloys Compd. 465 (2008) 375.
[21] K.M. Shaju, P.G. Bruce, Adv. Mater. 18 (2006) 2330.
[22] H.L. Chen, C.P. Grey, Adv. Mater. 20 (2008) 2206.
[23] R. Cabanel, G. Barral, J.P. Diard, B. Le Gorrec, C. Montella, J. Appl. Electrochem. 23 (1993) 92.